Materials Today Communications 51 (2026) 114679

Contents lists available at ScienceDirect

Materials Today Communications

journal homepage: www.elsevier.com/locate/mtcomm

Structural and mechanical properties of sodium stearate in glycol–water mixtures: Implications of composition

Mihail T. Georgiev [a,b,*], Ralitsa I. Uzunova [a,b], Theodor D. Gurkov [a], Ophelie Torres [c], Emily Cross [c]

[a] Department of Chemical and Pharmaceutical Engineering, Faculty of Chemistry and Pharmacy, Sofia University, Sofia 1164, Bulgaria
[b] "Smart Mechatronics, Eco- and Energy Saving Systems and Technologies", Sofia 1164, Bulgaria
[c] Unilever Research & Development Port Sunlight, Bebington CH63 3JW, UK

ARTICLE INFO

Keywords:
Sodium stearate
Propylene glycol
Dipropylene glycol
Rheology
SAXS
Mechanical properties
Yield stress

ABSTRACT

This study examines the composition–structure–property relationships of sodium stearate (NaST) formulations in propylene glycol and dipropylene glycol (PG/DPG)–water systems, focusing on the interplay between NaST concentration, water content, and mechanical performance. Using rotational rheometry, small-angle X-ray scattering (SAXS), and mechanical testing, we demonstrate that water increases yield stress; rather than acting as a plasticizer, it promotes a jammed lamellar network. SAXS shows lamellar order persists across compositions and up to 60 °C, with partial melting above this. At the same time, mechanical tests reveal a transition from ductile to plastic-elastic behavior as NaST concentration increases. The formulations at 8–10 wt% NaST exhibit maximum stiffness, toughness, and ultimate strength, making them promising for high-durability applications in personal care and pharmaceutical products. These findings provide a framework for designing NaST-based materials with tailored mechanical and structural properties.

1. Introduction

Sodium stearate (NaST) is a widely used surfactant and emulsifying agent with broad applications across cosmetics and personal care products, pharmaceuticals, and advanced systems [1–8]. It is well established that NaST forms lamellar liquid crystalline phases in aqueous environments, which strongly influence the system's rheological and mechanical properties. In particular, the lamellar network contributes to viscoelasticity and yield stress behavior–features essential for the stability and performance of soft-solid systems. Notably, the characteristics of these lamellar structures are highly sensitive to the NaST/stearic acid ratio, which plays a critical role in modulating the microstructure and phase behavior of the system [9].

Prior studies on NaST in water/co-solvent systems have shown that solvent composition strongly influences the lamellar microstructure. Liang et al. observed that at low NaST concentrations (1–5 wt%) in water/propylene glycol (PG) mixtures, water-rich samples form long lamellar fibers (ribbon-like crystallites), whereas PG-rich samples favor plate-like lamellar crystallites [10]. Notably, both morphologies share the same layered (lamellar) molecular structure. A decrease in overall solvent polarity (increasing PG content) induced a clear fiber-to-plate transformation, which was accompanied by corresponding changes in rheology. Thus, water content–and by extension the co-solvent fraction can modulate the NaST lamellar network architecture and its mechanical properties.

Beyond morphology, co-solvents such as propylene glycol also influence the crystallization behavior of NaST, promoting the formation of distinct lamellar polymorphs (e.g., α- and β-NaST) with varying rigidity and thermal stability [11].

Structural modifications in NaST-based systems directly influence key material properties such as hardness, yield stress, and viscoelasticity. As discussed, changes in solvent composition can alter lamellar morphology–from fibrous to plate-like structures–as well as the formation of specific lamellar polymorphs with distinct rigidity and thermal behavior [10,11]. These microstructural shifts are intimately linked to the system's mechanical performance. Notably, while water is conventionally regarded as a plasticizer, small amounts can counterintuitively increase yield stress by promoting jammed states, where water acts as a bridging phase between NaST lamellae [10]. This phenomenon underscores a complex and underexplored interplay between solvent

* Corresponding author at: Department of Chemical and Pharmaceutical Engineering, Faculty of Chemistry and Pharmacy, Sofia University, Sofia 1164, Bulgaria.
E-mail address: mtg@lcpe.uni-sofia.bg (M.T. Georgiev).

https://doi.org/10.1016/j.mtcomm.2026.114679
Received 2 October 2025; Received in revised form 4 December 2025; Accepted 13 January 2026
Available online 14 January 2026

polarity, co-solvent content, and NaST concentration in determining both the microstructure and the rheological response of the system.

Despite the relevance of NaST-based lamellar systems in soft matter research, a comprehensive understanding of how NaST concentration and water content jointly govern lamellar stability and mechanical behavior in glycol–water environments remains limited. While previous studies have explored the individual effects of water or specific glycols, the combined influence of multiple polyols–such as dipropylene glycol (DPG) and propylene glycol (PG)–in the presence of NaST has not been systematically investigated. We hypothesize that water, rather than acting solely as a plasticizer, contributes to the formation of jammed lamellar networks that enhance yield stress, and that this effect is modulated by NaST concentration and the presence of glycols. Unraveling this multicomponent interplay is essential for elucidating the physical mechanisms driving lamellar assembly, phase stability, and viscoelastic behavior.

Despite prior studies exploring NaST in water/PG systems at low concentrations, the combined effects of NaST concentration, water content, and the use of multiple glycols (PG and DPG) on the structural and mechanical properties of lamellar systems remain unexplored. In particular, there is no systematic investigation of how these variables interact to control yield stress, toughness, and structural transitions, especially in soft-solid regimes relevant to real-world formulations.

Moreover, while NaST is known to form lamellar phases, the role of water as a jamming agent, rather than a simple plasticizer, and the quantitative link between lamellar structure and mechanical behavior have not been clearly established.

We hypothesize that water promotes yield stress through lamellar jamming, and that this effect is modulated by NaST concentration. By combining rheology, SAXS, and mechanical compression testing, we aim to establish clear composition–structure–property relationships in these systems.

In this study, we investigate the structural and mechanical properties of NaST dispersions in propylene glycol and dipropylene glycol/water mixtures across a range of NaST concentrations and water contents. By integrating rheological measurements with small-angle X-ray scattering (SAXS), we demonstrate that increased water content can enhance yield stress through a jamming transition, while preserving lamellar organization across diverse compositional and thermal conditions. These findings provide mechanistic insight into how solvent composition and surfactant loading cooperatively determine the structure–property relationships in NaST-based lamellar systems.

2. Materials and methods

2.1. Materials

The experiments utilized analytical-grade sodium stearate (NaST) and stearic acid, both procured from Sigma-Aldrich. Dipropylene glycol and propylene glycol are both procured from TCI. Deionized water from the Millipore system (Milli-Q purification system) was used to prepare all solutions in the present study. All chemicals were used as received without further purification.

2.2. Preparation of NaST solutions

A stock glycol solution, composed of propylene glycol and dipropylene glycol in a 4.5 : 8 wt ratio, was prepared in advance for use in all subsequent solution preparations. For simplicity, this mixture is referred to as "glycols" throughout the text. Solutions were prepared by dissolving predetermined amounts of NaST in a blend of glycols and water to achieve concentrations ranging from 1 to 15 wt%. The solutions were uniformly heated for 30 min at 80 °C with constant stirring to ensure complete dissolution, then cooled to ambient temperature.

To investigate the influence of stearic acid on the system, select samples were prepared with stearic acid concentrations ranging from 0.5 to 2.0 wt%.

The samples were categorized based on the weight fraction of water relative to the total weight of the liquid phase, defined as $S = n_w / (n_w + n_g)$, where n_w is the weight fraction of water, n_g is the weight fraction of glycols, and n_s is the weight fraction of NaST. The total weight fraction of the dispersion satisfies the condition: $n_w + n_g + n_s = 1$, representing the total weight fraction of all ingredients. This systematic classification facilitates the analysis of rheological properties in relation to water content across the different formulations.

2.3. Rheological measurements

The rheological measurements were carried out using a rotational rheometer (Bohlin Gemini, Malvern, UK) equipped with a parallel-plate geometry, where the upper plate was rotational and the lower plate remained stationary, with a disk radius of $R = 20$ mm. The suspension was placed between the plates with a 2 mm gap, chosen to ensure uniform deformation across the sample. This was particularly important at higher NaST concentrations, where gel-like structures can produce deformation zones approaching or exceeding 0.5 mm. The larger gap minimized shear zone overlap, improved reproducibility, and ensured stable measurements across all compositions. Measurements were performed at 40 °C using controlled-stress mode, with shear stress applied in stepwise increments. At each stress level, the corresponding strain was recorded after reaching steady-state deformation, and flow curves were constructed accordingly.

2.4. Small-angle X-ray scattering (SAXS) analysis

The microstructure of the NaST solutions was characterized using SAXS with a Xenocs Xeuss 3.0 SAXS system. The instrument was equipped with a Cu Kα radiation source ($\lambda = 1.54$ Å). Scattering patterns were recorded over a q-range of 0.01–0.3 Å^{-1} at room temperature to assess the structural organization of the samples. To evaluate the thermal stability of the lamellar structures within the NaST solutions, samples were heated from 20 °C to 80 °C at a controlled rate of 2 °C/min. Measurements were taken at 10 °C increments to monitor changes in lamellar spacing and overall structural integrity.

2.5. Mechanical testing

Mechanical properties were evaluated via uniaxial compression tests using a Devotrans 50 kN testing machine with a load cell of 500 N. Cylindrical samples, each with a diameter of 20 mm and a height of 20 mm, were prepared for testing. Compression tests were conducted at a constant strain rate of 1 mm/min, with the samples deformed up to 50 % of their initial height (corresponding to a 10 mm). Load-displacement curves were recorded to analyze the mechanical behavior of the samples. All measurements were performed in triplicate, and the reported values represent average results; the standard deviation across samples was approximately 20 %.

3. Results and discussion

3.1. Rheological behavior

The rheological properties of NaST in mixed glycol solutions were investigated using a stress-controlled rotational rheometer at 40 °C. At each imposed shear stress (τ), the resulting strain (γ) was measured (Fig. 1a). In the low-stress regime (100–1000 Pa), γ increases steadily with τ and follows a power-law relationship when plotted on double-logarithmic axes ($\gamma \propto \tau^{\nu}$), yielding an average exponent of $\nu \approx 1.014 \pm 0.174$. This near-unity exponent indicates an approximately elastic-like response where strain is directly proportional to applied stress. Above 1000 Pa, ν deviates from 1, marking a quasi-elastic region likely involving microstructural rearrangements under shear [12].

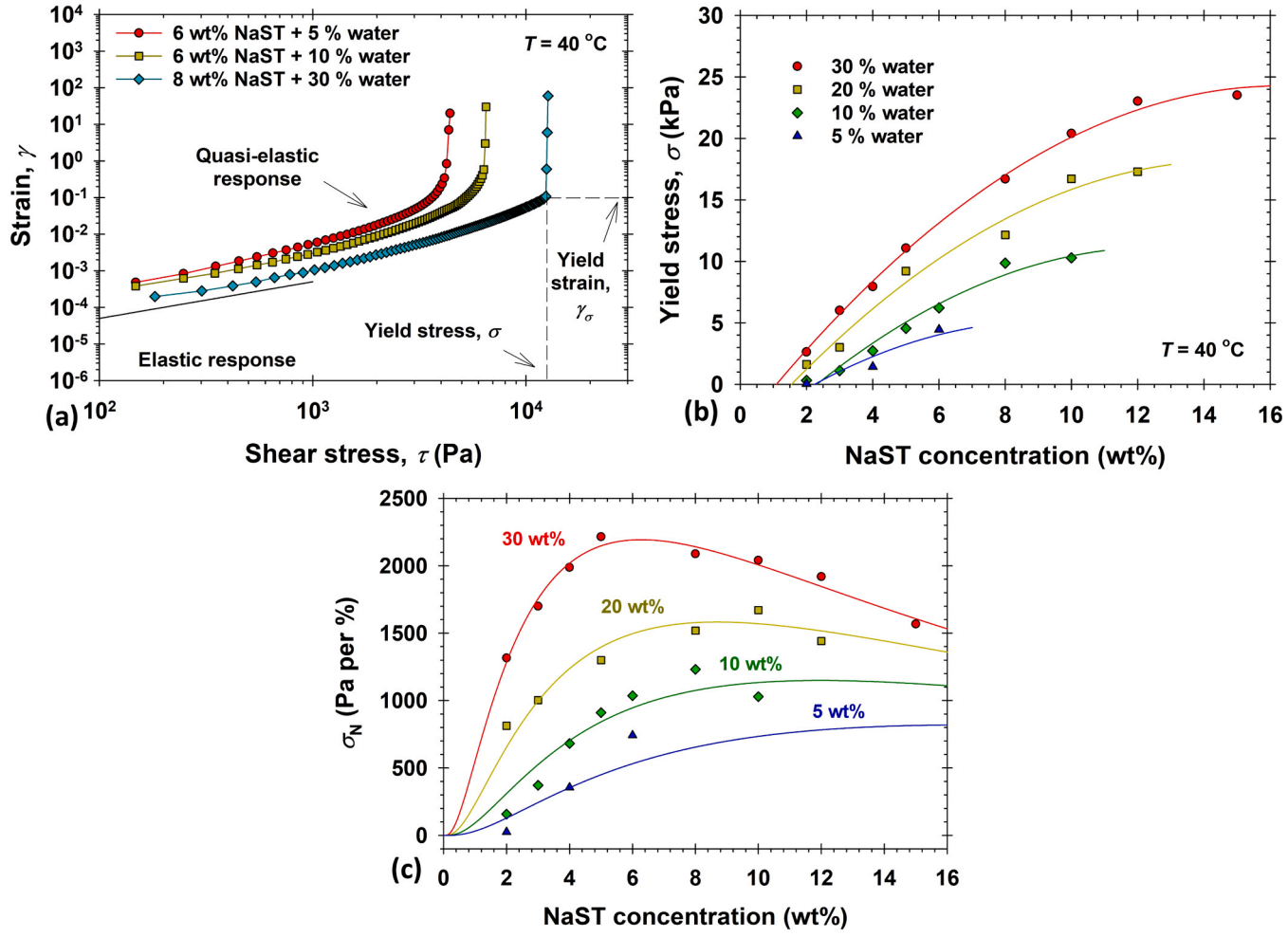

Fig. 1. Rheological behavior of NaST and glycols/water mixtures at 40 °C. (a) Strain response to shear stress at various NaST concentrations and water contents, showing regions of elastic and quasi-elastic behavior and highlighting the yield stress (σ). (b) Variation of yield stress with NaST concentration for different water contents, fitted with the global quadratic polynomial equation. (c) Normalized yield stress as a function of NaST concentration, modeled by a Gaussian-type (log-normal) function.

Upon surpassing a critical stress $\tau = \sigma$, the strain rises sharply, signifying the limit of elastic behavior. This critical stress σ is defined as the yield stress, and the corresponding strain is termed the yield strain (γ_σ). Here, σ was measured systematically for NaST concentrations (n_s) ranging from 1 wt% to 10 wt% at water contents (n_w) of 5, 10, 20, and 30 wt%.

As shown in Fig. 1b, the yield stress increases with n_s, which is consistent with a denser lamellar or soap-gel network that provides greater resistance to flow. Notably, σ also increases with higher n_w, challenging the conventional view of water as a simple plasticizer. For instance, at $n_s = 10$ wt%, σ rises from about 10280 Pa ($n_w = 10$ wt%) to 20400 Pa ($n_w = 30$ wt%), suggesting that water enhances the jammed suspension rather than diluting it. This effect can be rationalized by partial immiscibility and the potential for water to form capillary bridges or hydrate and reinforce the NaST lamellar framework, thereby stabilizing and strengthening the network. While water often softens many polymeric or surfactant-based systems, in these NaST/glycols/water mixtures, it appears to promote network connectivity and increase the yield stress. This observation supports the notion that NaST/glycols/water systems exhibit counterintuitive jammed suspensions.

To quantify these trends, the yield-stress data were fitted with a global quadratic polynomial equation (Eq. 1): $\sigma = \sigma_0 + \alpha x + \beta x^2$, where x is the NaST concentration (wt%), σ_0 and α are set-specific parameters for each water content, and β is a shared global parameter representing the curvature across all data sets. This empirical fit was used solely as a guide to the eye, without implying mechanistic significance. It captures the smooth, nonlinear increase in yield stress with concentration and enables visual comparison across compositions and hydration levels. The resulting curves (Fig. 1b) closely follow the experimental points and highlight the consistent curvature in the data.

To assess and compare the efficiency of sodium stearate across formulations with varying water content, the yield stress (σ) was normalized by the NaST concentration (n_s) to obtain a concentration-normalized yield stress $\sigma_N = \sigma/n_s$. This normalization allows direct comparison of reinforcement efficiency per unit NaST and facilitates identification of optimal loading levels beyond which additional NaST results in diminishing mechanical gains.

The normalized data were fitted using a log-Gaussian function defined on a logarithmic concentration scale:

$$\sigma_N = \frac{a}{n_s}\exp\left[-0.5\left(\frac{\ln(n_s/n_{s,0})}{b}\right)^2\right], \quad (2)$$

where a is a shared amplitude parameter representing the maximum theoretical efficiency, b controls the breadth of the log-Gaussian response, and $n_{s,0}$ is the characteristic NaST concentration at which the normalized yield stress profile is centered. In this work, a and b were treated as global fitting parameters across all samples, while $n_{s,0}$ was allowed to vary independently for each water content. This approach minimizes the number of free parameters while preserving the distinct

optimal behavior of each formulation.

While Eqs. (1) and (2) are used as empirical fitting models, they also offer insight into the underlying physical behavior of the system. Equation (1), the quadratic polynomial equation, reflects the tendency of the yield stress to approach a maximum value at high NaST concentrations, consistent with network densification and jamming phenomena observed in soft matter systems.

Eq. (2), the log-Gaussian function, captures the existence of an optimal concentration window for NaST efficiency, beyond which further addition provides diminishing or even adverse effects on normalized mechanical performance. The parameter a represents the peak normalized yield stress (i.e., the maximum reinforcement efficiency), $n_{s,0}$ identifies the NaST concentration at which this peak occurs, and b defines the width of the distribution, reflecting how sharply the efficiency drops outside the optimum range. Although not derived from first principles, the functional form mimics the behavior typical of many jammed or self-assembled systems, where performance emerges from a non-monotonic balance of interparticle interactions, packing density, and solvent-mediated effects.

From this model, the position of peak normalized yield stress and the corresponding concentration for each formulation can be calculated analytically as: $\sigma_{N,peak} = \frac{a}{n_{s,0}} e^{b^2/2}$, $n_{s,peak} = n_{s,0} e^{-b^2}$. The $\sigma_{N,peak}$ represents the maximum normalized yield stress, indicating the maximum material's resistance to flow, while $n_{s,peak}$, corresponds to the concentration at which this maximum occurs.

The resulting peak positions are summarized in Table 1. Notably, the formulation with 30 % water exhibited the highest normalized efficiency, with a peak at $n_{s,peak}$= 6.3 % and $\sigma_{N,peak}$= 2208 Pa/%, whereas the 5 % water system reached its peak at a substantially higher concentration of $n_{s,peak}$= 15.1 %, but with lower peak efficiency ($\sigma_{N,peak}$=912 Pa/%). These trends underscore the dual effect of water content: increasing water not only reduces the optimal NaST concentration required to achieve maximum reinforcement efficiency but also enhances the yield stress delivered per unit NaST at that optimum.

This behavior can be explained by considering water's role as a physical jamming agent. At optimal NaST concentrations, added water encourages stronger lamellar stacking, thereby increasing structural rigidity. Instead of simply acting as a plasticizer, water here results in tighter packing and limits bilayer mobility, which enhances the network's load-bearing capacity. This leads to a higher yield stress despite the dilution effect, especially when the lamellar domains remain sufficiently connected to transmit mechanical stress.

3.2. SAXS analysis

Fig. 2a presents the SAXS patterns of NaST solutions with a fixed water content (n_w = 30 wt%) at increasing NaST concentrations. The background scattering profile, collected without any sample, is included for reference. These patterns are raw and encompass both the liquid phase and any dispersed structures within the sample. Across the entire range of NaST concentrations (1 wt% to 8 wt%), a lamellar phase is consistently observed, as evidenced by harmonic peaks at qL, $2qL$, $3qL$, etc., reflecting a stable liquid-crystalline arrangement.

In the 1–5 wt% NaST range, the 2D patterns exhibit arc-like powder rings (Fig. 2a, arrows) consistent with crystalline stearic acid—either a common residual from NaST manufacture or the result of partial protonation of stearate during sample preparation (e.g., CO_2 uptake/acidification). Above 4 wt% NaST, the intensity of these rings progressively declines. By 5 wt%, only a faint residual signal remains, consistent with near-complete uptake of stearic acid by the lamellar NaST phase (via dissolution or incorporation into mixed lamellae).

The dominant lamellar architecture, indicated by primary peaks at approximately 0.14, 0.28, and 0.42 $Å^{-1}$, remains unchanged as the NaST concentration increases. The additional peaks at lower q-values correspond to the stearic acid crystallites [13]. The constancy of the main lamellar peak positions across this concentration range affirms the structural integrity and uniformity of the lamellar phase. These findings support the conclusion that the observed variations in normalized yield stress (σ_N), as shown in Fig. 1b, stem primarily from collective bulk phenomena rather than from significant alterations at the microstructural level.

Fig. 3a shows the effect of stearic acid on the microstructure of an 8 wt% NaST solution containing 30 wt% water. The baseline SAXS pattern, recorded in the absence of additional stearic acid, lacks the characteristic low-q peaks associated with crystalline stearic acid. Incremental additions of stearic acid (0.2 wt%, 0.8 wt%, and 1.6 wt%) progressively introduce asymmetric scattering features in the 2D SAXS images, accompanied by a corresponding increase in low-q peak intensity (Fig. 3b). These observations confirm the distinctive scattering signature of stearic acid within the NaST formulation.

This apparent correlation is critical for distinguishing the microstructural characteristics imparted by stearic acid from those inherent to the NaST/glycols/water mixture. The emergence of asymmetric scattering signals and enhanced low-q peaks demonstrates the progressive integration of stearic acid into the lamellar framework. These findings reinforce the proposed microstructural interpretation of the NaST/stearic acid/glycol/water system, linking the microscopic assembly to macroscopic rheological properties, such as the yield stress trends reported in Fig. 1b.

In addition to compositional effects, the thermal stability of the lamellar structure was investigated for an 8 wt% NaST formulation. As shown in Fig. 4, the SAXS intensity profiles indicate that the lamellar liquid-crystalline state is preserved up to 60 °C, highlighting its robust resistance to thermal fluctuations. Above this temperature, partial melting and loss of order become evident at 70 °C, signaling the thermal limit of structural stability.

3.3. Mechanical properties

To fully understand the macroscopic behavior of soft, structured materials, it is essential to combine structural, rheological, and mechanical characterization. While rheological tests at elevated temperatures reveal shear response and gel strength, and SAXS clarifies nanoscale ordering, mechanical compression testing examines bulk deformation resistance and fracture behavior. This section presents such compression tests to enhance and deepen the understanding of how microstructure and hydration influence the material's load-bearing capabilities.

3.3.1. Compression testing

Fig. 5 presents sequential images illustrating the mechanical

Table 1
Fitting parameters obtained from Eqs. (1) and (2).

n_w (wt%)	σ_0 (kPa)	α(kPa/%)	β (kPa/%^{2})	a (kPa·%)	b (-)	$n_{s,0}$ (%)	$n_{s,peak}$ (%)	$\sigma_{N,peak}$ (Pa/%)
5	-3.82	1.94	-104.82	24.8	1.082	48.9	15.1	912
10	-5.56	2.65				38.4	11.9	1160
20	-4.52	3.09				28.0	8.7	1594
30	-3.61	3.42				20.2	6.3	2208

Note: Standard errors are ~14 % of the fitted values for most parameters; the 5 %-water amplitude shows a higher value of ~29 %.

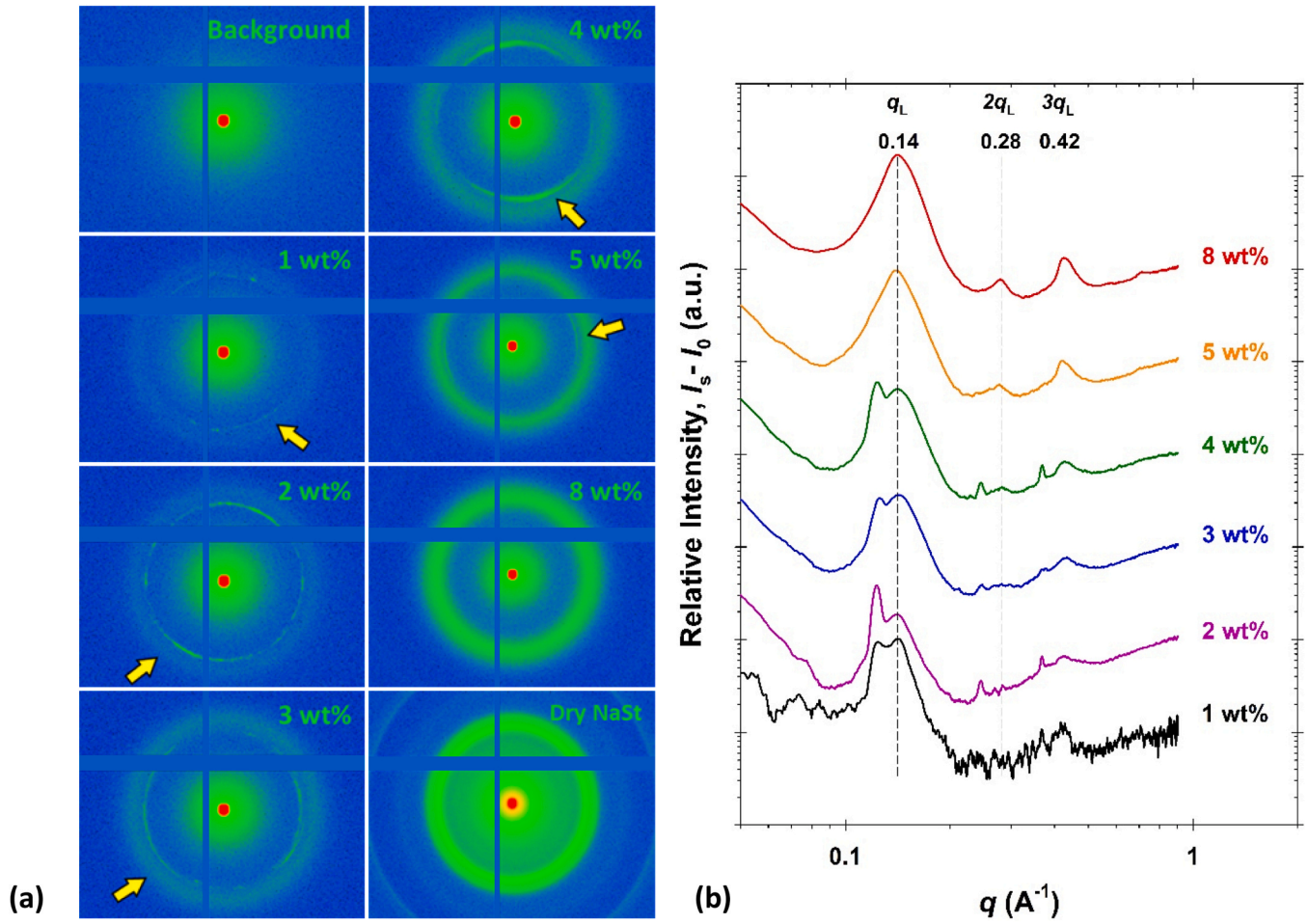

Fig. 2. SAXS analysis of NaST solutions at $n_w = 30$ wt% at 25 °C. (a) 2D SAXS patterns for NaST solutions at various concentrations. Arrows point to the additional scattering features emerging from anisotropic signal. (b) Relative scattering intensity profiles as a function of scattering vector, with characteristic peaks revealing the presence of ordered structures at different NaST concentrations.

compression behavior of cylindrical NaST blocks (radius: 10 mm; height: 20 mm) under increasing compressive stress. Deformation is recorded at 0 %, 10 %, 30 %, and 50 % compression levels to capture the material's response visually. At 10 % deformation, liquid expulsion from the block becomes evident, indicating the initial structural response to applied stress. During compression, liquid is gradually expelled from the sample, indicating a continuous breakdown of the NaST structure as the deformation progresses.

At 50 % deformation, the block exhibits visible fracturing, marked by sharp drops in the load-displacement curve. This point of failure delineates the mechanical threshold beyond which the structural network can no longer sustain stress. Identifying this transition is key to understanding the limits of mechanical resilience in soft solids and gels, particularly in maintaining integrity under sustained compressive strain.

3.3.2. *Tensile test observations*

As shown in Fig. 6a, the load-displacement curve for a cylindrical block of 8 wt% NaST + 30 wt% water exhibits a plastic-elastic behavior, capturing the critical transition point at which the material yields and begins to deform plastically. This curve is pivotal for understanding how the formulation responds to stress and how it sustains permanent deformation without forming cracks.

In Fig. 6b, the stress–strain curve illustrates the approach used to determine the elastic modulus before and after the yield point, as well as the yield stress. The initial modulus (E_1) quantifies the material's stiffness in response to small deformations, while the post-yield modulus (E_2) describes the decreased stiffness once yielding has begun. This latter phase underscores the material's altered mechanical properties under continued loading after yield.

The total toughness of each specimen, as shown in Fig. 6c, was quantified by integrating the area under the load-displacement curve from zero extension to the maximum displacement tested (10 mm). This approach captures the entire energy-absorbing capacity of the material under tensile loading, including post-crack behavior, provided the sample continued to sustain load. Abrupt load drops corresponding to crack initiation and propagation were included in the analysis, as these do not necessarily represent catastrophic failure or complete loss of load-bearing capacity. For each block, both the resulting total work (N·mm) and the intrinsic toughness, calculated as total work normalized by the sample volume (mJ/mm^3), are reported in Table 2, allowing direct comparison across all tested NaST concentrations at fixed water content (30 wt%).

For reference, the ultimate strength is indicated in Fig. 6d, typically occurring at a displacement of 5.5–9.0 mm, depending on composition. As demonstrated in the representative load-displacement curve (Fig. 6d), the onset of visible cracking is accompanied by only a moderate reduction in load (generally less than 50 % of the peak value), indicating that the specimens retain substantial post-crack load-bearing capacity. This behavior justifies using total work (up to 10 mm of displacement) as a meaningful metric for energy absorption, as the material continues to sustain significant load even after crack formation. The full set of mechanical parameters, including pre-yield elasticity (E_1), post-yield elasticity (E_2), yield strength, total toughness, and intrinsic toughness, is summarized in Table 2.

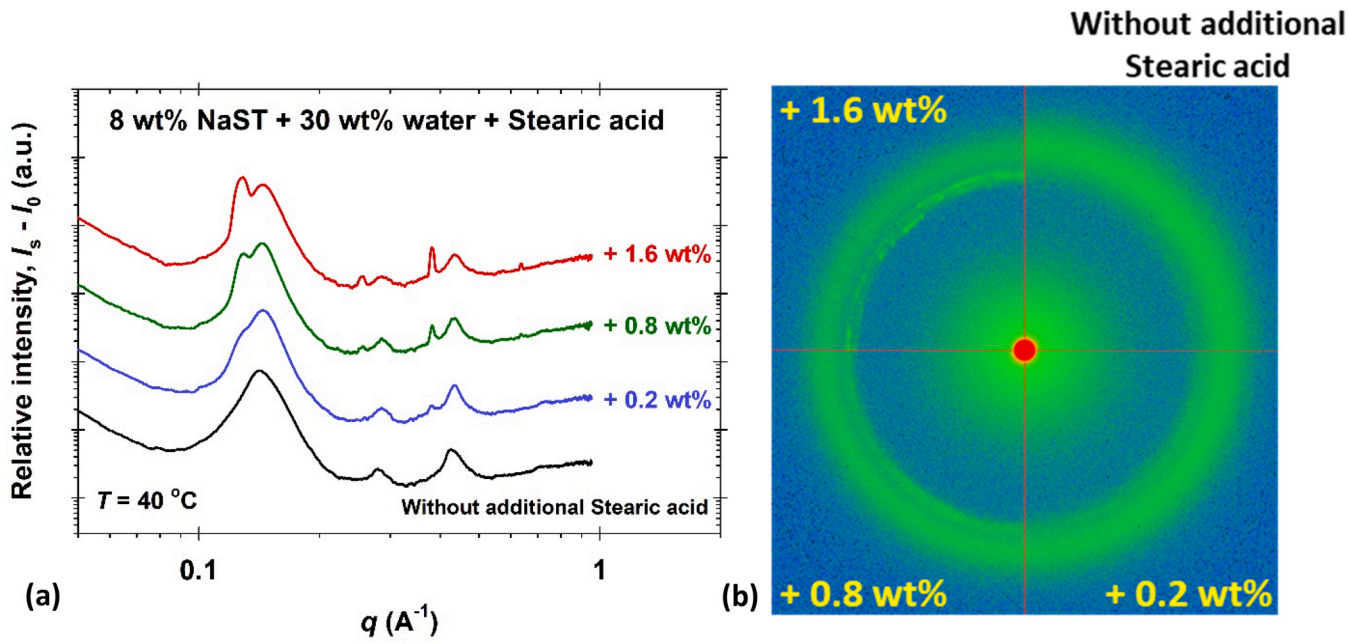

Fig. 3. Effect of stearic acid on the structure of NaST solutions. (a) SAXS intensity profiles for an 8 wt% NaST solution with 30 wt% water at 40 °C, with varying concentrations of added stearic acid. The appearance of a small peak indicates the formation of stearic acid crystals. (b) SAXS pattern demonstrating anisotropic features, confirming the crystalline nature of the added stearic acid.

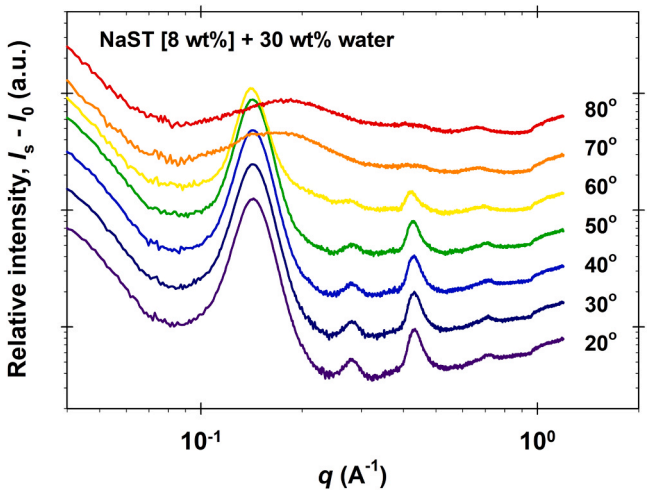

Fig. 4. Temperature stability of the lamellar structure of the NaST/glycols/water mixture. SAXS intensity profiles of an 8 wt% NaST solution with 30 wt% water measured at different temperatures ranging from 20 °C to 80 °C.

3.3.3. *Mechanical properties and concentration dependence*

Fig. 7a shows the load-displacement curves for NaST samples with a constant 30 wt% water content across a spectrum of NaST concentrations ranging from 3 wt% to 10 wt%. This graph provides a quantitative measure of the material's mechanical strength and elasticity as it deforms. As the concentration of NaST increases, the curves become progressively steeper, indicating that a higher load is required to achieve the same degree of displacement. This behavior is particularly apparent in samples with higher NaST concentrations, which exhibit greater resistance to deformation, as evidenced by their higher slope curves on the graph. The curve for the 3 wt% concentration shows a relatively gentle slope, suggesting that this sample is the most pliable and can undergo greater displacement before reaching the same load level as its higher-concentration counterparts. Conversely, high concentrations (9 and 10 wt%) exhibit a steeper initial slope, indicating a material that is significantly stiffer and offers greater resistance to deformation.

These load-displacement curves are instrumental in evaluating the toughness of the NaST samples. The area under each curve, up to the point of material breakage, represents the amount of energy the material can absorb before failing, which is a key parameter in the design and application of these materials, where mechanical reliability is crucial. Furthermore, the initial portion of the curves - before the yield point - provides insight into the material's elastic modulus, an indicator of stiffness. As NaST content rises, so does the sample's stiffness, up to the

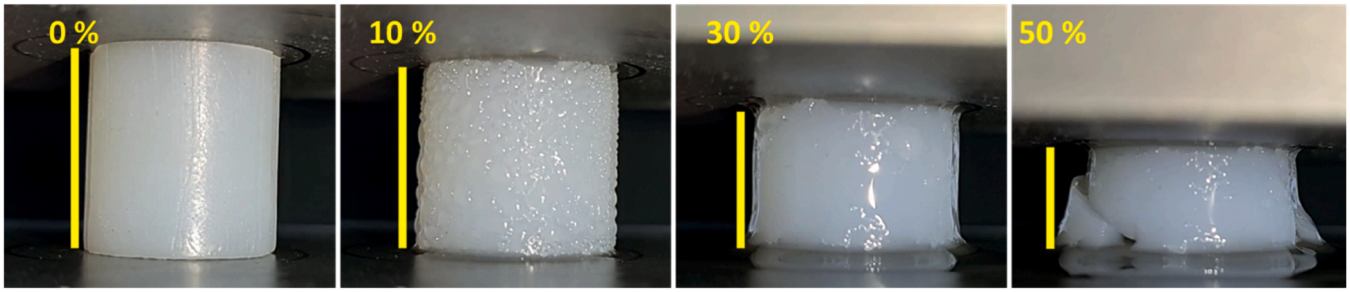

Fig. 5. Sequential images of a cylindrical block of 8 wt% NaST + 30 wt% water at varying degrees of mechanical compression. The yellow lines indicate the level of compression: 0 % (initial state), 10 %, 30 %, and 50 %.

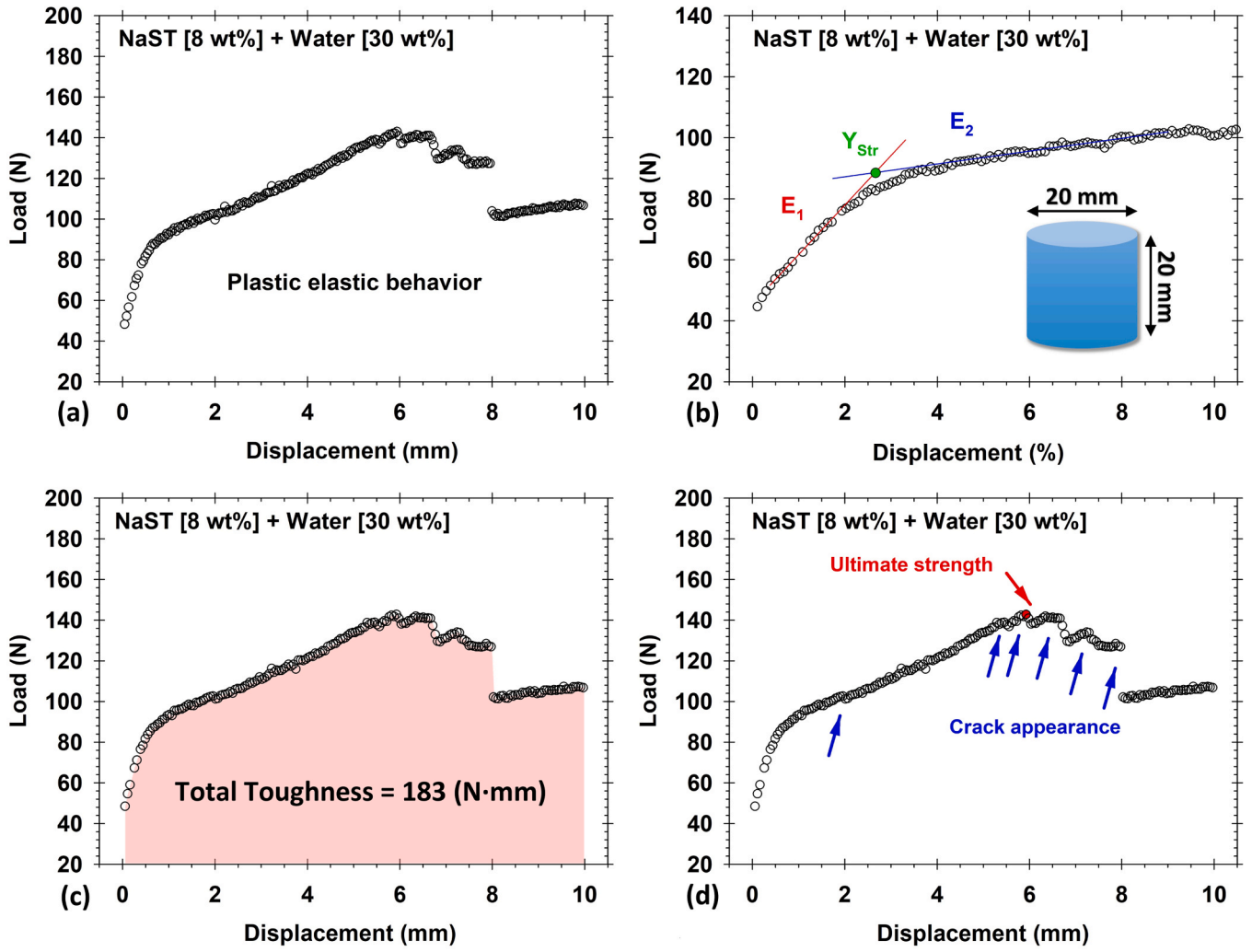

Fig. 6. Detailed analysis of mechanical behavior under uniaxial compression for an 8 wt% NaST solution with 30 wt% water. (a) The load-displacement curve demonstrates a plastic–elastic response. (b) The stress–strain curve with annotations for the moduli of elasticity (E_1, E_2) and yield strength (Y_{str}). (c) The shaded area under the load-displacement curve (pink) represents the total toughness. (d) A detailed view of the load–displacement curve showing ultimate strength and crack initiation leading to failure.

Table 2
Mechanical properties for NaST formulations with 30 wt% water.

n_s(wt %)	E_1 (N/mm)	E_2 (N/mm)	Y_{Str} (N)	Total Toughness (N·mm)	Intrinsic Toughness (MPa)
3	37.6	0.9	19.6	44.1	7.0
4	43.5	0.6	27.0	77.4	12.3
5	47.7	0.8	35.0	99.2	15.8
6	46.5	2.0	51.6	124.0	19.7
7	50.4	3.7	71.1	162.3	25.8
8	57.9	8.4	70.0	183.0	29.1
9	106.9	10.7	32.1	259.0	41.2
10	94.0	17.9	27.0	252.5	40.2

yield point, after which plastic deformation begins, and the material behavior changes.

In Fig. 7b, the transition from ductile to plastic-elastic behavior is evident. For concentrations ranging from 3 to 7 wt%, the curves exhibit characteristics of ductile behavior, where the material deforms significantly before reaching failure [14]. In this regime, the yield stress is determined by the peak of the curve. As the NaST concentration escalates from 8 to 10 wt%, a shift towards plastic-elastic behavior is happening. This behavior is typified by the curve's intersection between the initial elastic slope and the subsequent plastic plateau, indicative of a material that becomes more compact and capable of withstanding higher loads post-yield.

The delineation between ductile and plastic-elastic behavior is critical, as the calculation of yield stress differs between the two. For ductile behavior, the yield stress corresponds to the maximum load before deformation, whereas, for plastic-elastic behavior, it is derived from the intersection of linear approximations representing the material's response at low and high strains. The tendency for ductile behavior observed between 3 and 7 wt% NaST concentrations suggests a structure with diminished strength post-yield when compared to the 8–10 wt% concentrations, which show a compacting structure able to endure greater loads after yielding. Comprehensive data from the analysis of all curves are presented in Table 2, elucidating the influence of NaST concentration on the mechanical response of the system.

Fig. 7c illustrates the methodology employed to analyze the mechanical properties of NaST formulations, bridging experimental observations from Figs. 7a and 7b with the data interpretation techniques used. This figure highlights the procedure for determining yield stress, marked as point C, and the distinct approach to calculate elasticity before and after this yield point for both ductile and plastic behavior regimes. The initial elastic modulus, E_i, representing the stiffness of the material before yielding, is calculated from the slope of the initial linear region of the curve, extending from point A to point B. This modulus is

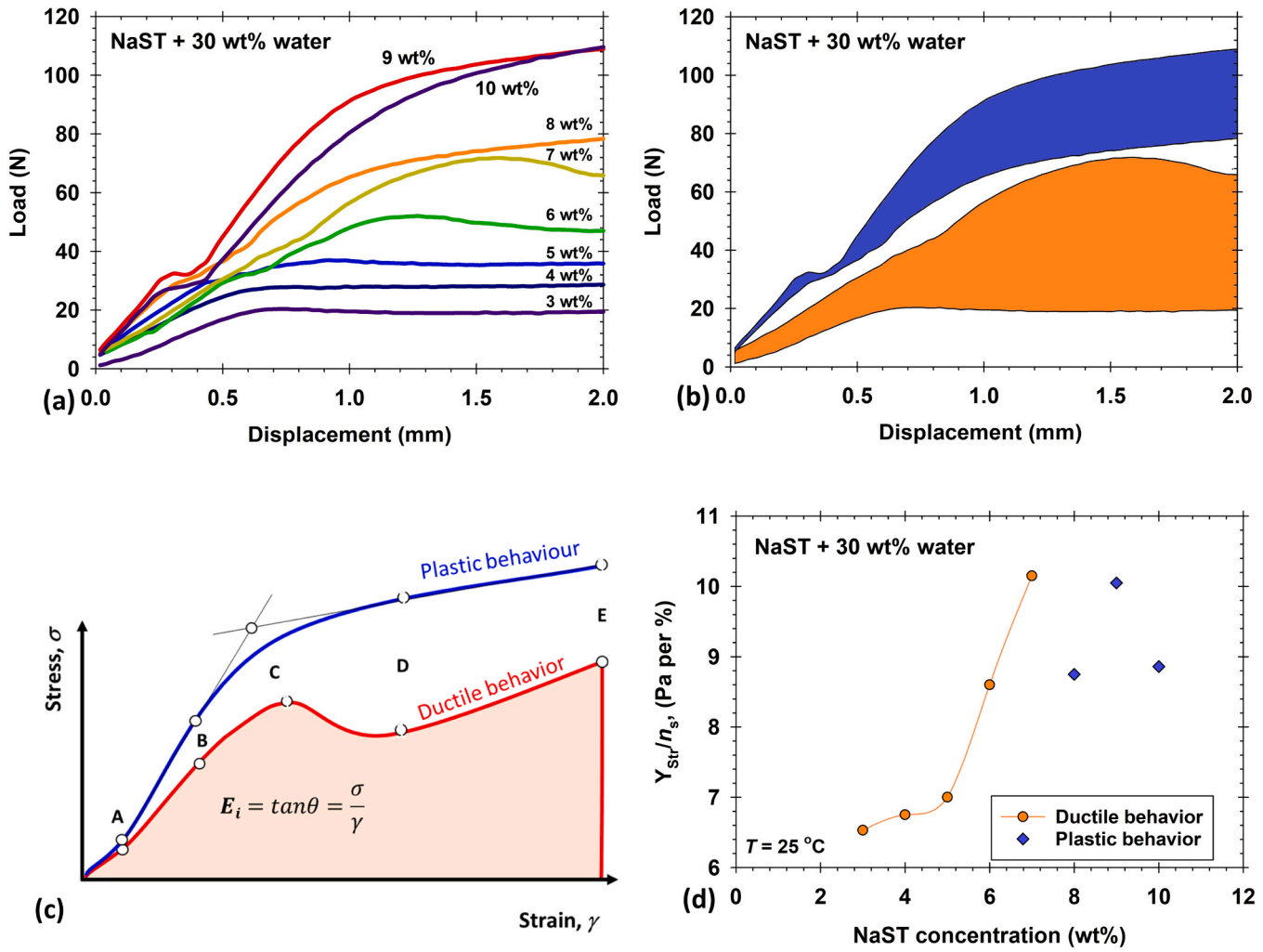

Fig. 7. Mechanical properties of NaST solutions. (a) Load-displacement curves for NaST solutions at various concentrations show increased resistance with increasing concentration. (b) Distinction between ductile and plastic-elastic behavior in NaST solutions. (c) Normalized yield stress plotted against NaST concentration, distinguishing ductile from plastic behavior. (d) Normalized Yield Stress in relation to NaST concentration.

mathematically expressed as:

$$E_i = \tan\theta = \frac{\sigma}{\gamma}, \tag{3}$$

where θ is the angle of the slope, σ is the stress, and y is the strain. After the yield point, the material's behavior transitions, reflecting its ability to absorb energy and deform without fracturing. The elasticity post-yield is determined by analyzing the curve from point D to E, where the material exhibits either a hardening or softening response, indicative of plastic behavior or enhanced ductility, respectively.

In Fig. 7d, the normalized yield stress data for NaST samples are presented in relation to NaST concentration. The graph illustrates the material's stress at yield, normalized by the concentration of NaST, providing an insightful metric for evaluating the influence of NaST content on the mechanical strength of the system. The plot reveals two distinct behavioral patterns: ductile (orange circles) and plastic (blue diamonds), corresponding to the deformation characteristics previously discussed. In the ductile regime, up to a NaST concentration of 7 wt%, there is a progressive increase in normalized yield stress, denoting a material that elongates substantially under stress before reaching its yield point. This indicates that the formulations become tougher with an increasing amount of NaST, able to absorb more energy during deformation.

Upon exceeding an 8 wt% concentration of NaST, the plot transitions to exhibit plastic behavior, where the normalized yield stress levels off. This plateau suggests that the material maintains its load-bearing capacity post-yield without significant further deformation, signaling a change in the material's internal structure that enhances its ability to bear stress. Conducted at 25 °C, the normalized yield stress analysis elucidates the material's structural behavior under compressive forces, which is fundamental for understanding its potential applications. Such insights into the yield stress are critical for understanding soft solids with precise mechanical properties that are capable of withstanding specific stress conditions without compromising their structural integrity.

4. Conclusions

This work reveals a direct composition–structure–property link in sodium stearate/glycol/water systems. Water, rather than acting as a conventional plasticizer, emerges as a network former, substantially increasing yield stress and toughness by promoting jammed, thermally stable lamellar architectures. SAXS confirms the persistence of ordered lamellar domains across a broad compositional and temperature range. Mechanical testing further identifies a concentration-dependent transition from ductile to plastic-elastic behavior, with peak total and intrinsic toughness achieved at 8–10 wt% NaST and 30 wt% water. Remarkably, these materials retain significant load-bearing capacity and energy

absorption even after visible crack formation.

These results provide a quantitative foundation for tuning mechanical properties in soft-matter systems by controlling co-solvent and surfactant concentration. The strong post-crack load retention and high toughness demonstrated here highlight the potential of NaST-based lamellar networks as robust, fracture-resistant soft solids. The composition-driven jamming transition and post-yield resilience uncovered in this study may inform the rational design of advanced materials where structural integrity and energy dissipation are essential.

Future investigations should address the dynamic recovery and self-healing behavior of these lamellar systems and extend these principles to related amphiphilic or fatty-acid salt materials. The insights gained here set the stage for further innovations in soft-matter science and functional materials engineering.

CRediT authorship contribution statement

Georgiev Mihail: Writing – review & editing, Writing – original draft, Visualization, Methodology, Formal analysis, Data curation. **Theodor D. Gurkov:** Writing – review & editing, Supervision, Project administration, Conceptualization. **Ralitsa I. Uzunova:** Investigation. **Emily Cross:** Resources, Funding acquisition, Conceptualization. **Ophelie Torres:** Resources, Funding acquisition, Conceptualization.

Funding

This work was partially supported by Unilever R&D Port Sunlight, UK.

Declaration of Competing Interest

The authors declare that they have no known competing financial interests or personal relationships that could have appeared to influence the work reported in this paper.

Acknowledgments

The authors are grateful to the European Regional Development Fund under the Operational Program “Research, Innovation and Digitalization for Smart Transformation 2021–2027”, Project BG16RFPR002–1.014–0005; Project BG16RFPR002–1.014–0006; and Project BG16RFPR002–1.014–0001.

Data availability

Data will be made available on request.

References

[1] C. Solans, M.J. García-Celma, Microemulsions and Nano-emulsions for Cosmetic Applications, in: Cosmetic Science and Technology, Elsevier, 2017, pp. 507–518, https://doi.org/10.1016/B978-0-12-802005-0.00029-X.
[2] J. Li, X. He, Y. Sun, R. Song, X. Ren, X. Zhang, J. Guan, S. Mao, Effect of lubricants type and particle size on the rheological properties and aerosolization behavior of dry powder inhalers, Int. J. Pharm. 667 (2024) 124911, https://doi.org/10.1016/j.ijpharm.2024.124911.
[3] H. Nie, W. Xu, J. Ren, L.S. Taylor, P.J. Marsac, C.T. John, S.R. Byrn, Impact of metallic stearates on disproportionation of hydrochloride salts of weak bases in solid-state formulations, Mol. Pharm. 13 (2016) 3541–3552, https://doi.org/10.1021/acs.molpharmaceut.6b00630.
[4] J. Yu, M.-C. Romeo, A.A. Cavallaro, H.-K. Chan, Protective effect of sodium stearate on the moisture-induced deterioration of hygroscopic spray-dried powders, Int. J. Pharm. 541 (2018) 11–18, https://doi.org/10.1016/j.ijpharm.2018.02.018.
[5] L.-S. Hao, C. Yuan, H.-L. Zhong, J.-W. Ling, H.-X. Wang, Y.-Q. Nan, Triple-stimuli-responsive hydrogels based on an aqueous mixed sodium stearate and cetyltrimethylammonium bromide system, J. Mol. Liq. 364 (2022) 120010, https://doi.org/10.1016/j.molliq.2022.120010.
[6] D. Li, H. Du, W. Guo, M. Chen, X. Guo, P. Li, Y. Zhou, P. Chen, M. Li, Y. Xu, Crosslinking of a polycaprolactone/tourmaline scaffold by sodium stearate with improved mechanical strength and bioactivity, RSC Adv. 13 (2023) 24519–24535, https://doi.org/10.1039/D3RA04273A.
[7] F. Jia, L. Chen, J. Zhang, Q. Hu, Y. Wang, Effect of sodium stearate modified waste marble powder on the properties and hydration of cement mortar, Constr. Build. Mater. 465 (2025) 140213, https://doi.org/10.1016/j.conbuildmat.2025.140213.
[8] Final Report of the Safety Assessment of Lithium Stearate, Aluminum distearate, aluminum stearate, aluminum tristearate, ammonium stearate, calcium stearate, magnesium stearate, potassium stearate, sodium stearate, and zinc stearate, Int. J. Toxicol. 1 (1982) 143–177. ⟨https://api.semanticscholar.org/CorpusID:208499512⟩.
[9] M. Heppenstall-Butler, M.F. Butler, Nonequilibrium behavior in the three-component system stearic acid−sodium stearate−water, Langmuir 19 (2003) 10061–10072, https://doi.org/10.1021/la034833p.
[10] J. Liang, Y. Ma, Y. Zheng, H.T. Davis, H.-T. Chang, D. Binder, S. Abbas, F.-L. Hsu, Solvent-induced crystal morphology transformation in a ternary soap system: sodium stearate crystalline fibers and platelets, Langmuir 17 (2001) 6447–6454, https://doi.org/10.1021/la001724r.
[11] J. Liang, Y. Ma, B. Chen, E.J. Munson, H.T. Davis, D. Binder, H.-T. Chang, S. Abbas, F.-L. Hsu, Solvent modulated polymorphism of sodium stearate crystals studied by X-ray diffraction, solid-state NMR, and Cryo-SEM, J. Phys. Chem. B 105 (2001) 9653–9662, https://doi.org/10.1021/jp010532h.
[12] M.T. Georgiev, K.D. Danov, P.A. Kralchevsky, T.D. Gurkov, D.P. Krusteva, L. N. Arnaudov, S.D. Stoyanov, E.G. Pelan, Rheology of particle/water/oil three-phase dispersions: Electrostatic vs. capillary bridge forces, J. Colloid Interface Sci. 513 (2018) 515–526, https://doi.org/10.1016/j.jcis.2017.11.057.
[13] C. Blach, A.J. Gravelle, F. Peyronel, J. Weiss, S. Barbut, A.G. Marangoni, Revisiting the crystallization behavior of stearyl alcohol: stearic acid (SO: SA) mixtures in edible oil, RSC Adv. 6 (2016) 81151–81163, https://doi.org/10.1039/C6RA15142F.
[14] M.A. Meyers, K.K. Chawla, Mechanical Behavior of Materials, 2nd ed., 2008.